methane

MDPI

Review

Research Progress on Stability Control on Ni-Based Catalysts for Methane Dry Reforming

Minghui Wei [1] and Xuerong Shi [1,2,*]

[1] School of Materials Engineering, Shanghai University of Engineering Science, Shanghai 201620, China; m350122104@sues.edu.cn
[2] National Key Laboratory of High Efficiency and Low Carbon Utilization of Coal, Institute of Coal Chemistry, Chinese Academy of Sciences, Taiyuan 030001, China
* Correspondence: shixuer05@mails.ucas.ac.cn

Abstract: CO_2 reforming of CH_4 (DRM) utilizes the greenhouse gases of CH_4 and CO_2 to obtain the synthesis gas, benefiting the achievement of carbon neutrality. However, the deactivation of Ni-based catalysts caused by sintering and carbon deposition limits the industrial application. Focusing on stability improvement, this review first summarizes the reaction mechanism and deactivation mechanism in DRM and then discusses the impact of catalyst active components, supports, and interfacial structure. Finally, we propose the design direction of stable Ni-based catalysts towards DRM, providing guidance for the future development of catalysts suitable for industrial production.

Keywords: methane dry reforming; Ni-based catalysts; deactivation; regulation

check for updates

Citation: Wei, M.; Shi, X. Research Progress on Stability Control on Ni-Based Catalysts for Methane Dry Reforming. *Methane* **2024**, *3*, 86–102. https://doi.org/10.3390/methane3010006

Academic Editors: Brian A. Rosen and Oz M. Gazit

Received: 17 November 2023
Revised: 13 December 2023
Accepted: 27 December 2023
Published: 6 February 2024

1. Introduction

Methane (CH_4) and carbon dioxide (CO_2) are two major greenhouse gases but also important carbon resources [1–4]. Catalytic conversion and utilization of these two greenhouse gases through chemical pathways is of positive significance for mitigating the greenhouse effect and closing the carbon cycle [5]. Additionally, CH_4 and CO_2 are important components of biogas, which come from a wide range of sources [6]. Methane dry reforming (DRM) can convert CH_4 and CO_2 into carbon-rich synthesis gas, which is particularly suitable for hydroformylation synthesis to fulfill the high-value utilization of biogas. DRM, which is strongly endothermic thermodynamically, needs to be performed under high temperature (700–1000 °C) conditions. On the one hand, this leads to high energy consumption, and on the other hand, there is catalyst deactivation caused by high-temperature sintering and carbon deposition. Therefore, how to improve the stability and low-temperature activity of the DRM catalyst has become the key to industrial application [7]. Among various metal-based DRM catalysts, the inexpensive earth-abundant Ni-based catalysts stand out because they show high catalytic activity, comparable to noble metals such as Ru and Rh [8]. However, Ni-based catalysts also deliver excellent C-H bond cleavage ability. The formed carbon species deposit on the Ni surface and form stable carbon structures, leading to the block of metal-active sites and inducing deactivation [9–12].

To understand and seek possible solutions to catalyst deactivation issues, this review first reveals the reaction mechanism and deactivation mechanism of DRM and then discusses the influence of catalyst active components, supports, and microenvironment. Finally, the development direction of stable DRM catalysts is proposed, which provides guidance for the design of catalysts suitable for industrial applications (Figure 1).

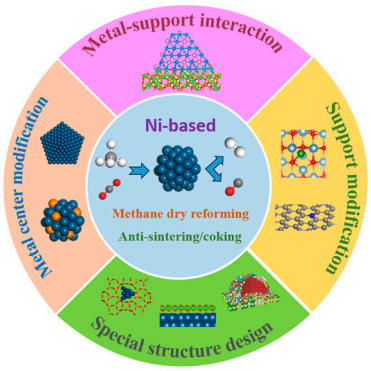

Figure 1. Illustration of DRM.

2. DRM Reaction Mechanism and Deactivation Mechanism

The reaction network of DRM is complex. The reaction (Entry 1), Table 1 is accompanied by side reactions such as the reverse water gas shift (RWGS) reaction (Entry 2) and carbon deposition reaction, including CH_4 dissociation (Entry 3), CO disproportionation, namely, the Boudouard reaction (Entry 4) and CO redox (Entry 5).

Table 1. Standard reaction enthalpy of reactions involved in DRM.

Entry	Elementary Step	ΔH^{θ} (kJ/mol)
1	$CO_2 + CH_4 \rightarrow 2H_2 + 2CO$	+247
2	$CO_2 + H_2 \rightarrow CO + H_2O$	+41
3	$CH_4 \rightarrow C + 2H_2$	+75
4	$2CO \rightarrow C + CO_2$	−172
5	$CO + H_2 \rightarrow C + H_2O$	−175

As can be seen from the above reaction equation, DRM is strongly endothermic, and a high temperature is required to promote the reaction. Due to the presence of the side reaction of (Entry 2), the $CO{:}H_2$ mole ratio is less than 1. Since the DRM reaction is carried out in the thermodynamic carbon deposition zone (Entry 3), it is impossible to improve the carbon deposition of the DRM reaction by changing the thermodynamic conditions of the reaction. Therefore, this review focuses on possible kinetic ways to increase the reaction rate of DRM while decreasing the reaction rates of side reactions by the adjustment of influencing factors.

2.1. Reaction Mechanism

The DRM mechanism has been extensively studied [13,14]. It is generally believed that DRM reactions on Ni-based catalysts follow these steps:

(1) Activation of CH_4. It generally occurs on the active site of the metal and at the interface between the metal and the support. CH_4 adsorbs on these active metal surfaces and gradually dissociates to C* or CH* [15–17].

(2) Activation of CO_2. The activation of CO_2 usually occurs on the support or at the interface between the support or the support rather than on metal. The obtained H from the CH_4 dissociation on Ni may assist CO_2 activation via COOH* or HCOO* species [18]. The rate-limiting step varies depending on the system. The dissociation of CH_4 on the catalyst is generally considered to be a rate control step for DRM [18]. M-O* species formed on metal surfaces after preferential activation of CO_2 can promote methane activation [19]. However, some studies have shown that CO_2 dissociation at high temperatures may be a rate-limiting step [20]. For bifunctional catalysts, such as Pd/ZrO_2, it is a multi-step-controlled reaction [21].

(3) Oxidation and decomposition of intermediates. C* or CH*, which is from the CH_4 dissociation, is oxidized by O* to produce CO* or CHO*, and then CHO* is decomposed

into CO* and H* [21]. The origin of O* is diverse, which could come from the decomposition of CO_2 or from the oxide support [22–24]. For those supports with high oxygen release capacity and lattice oxygen mobility, such as La_2O_3 [23] and CeO_2 [23], direct oxidation of CH_x species by the lattice oxygen ($O_{lattice}$) via a Mars−van Krevelen-type redox mechanism is proposed. In this mechanism, the active carbon intermediates from methane dissociation are oxidized directly by the lattice oxygen of the support to form CO and oxygen vacancies, avoiding the formation of carbon species on the Ni surface [23]. The oxygen vacancies then serve as the activation sites for CO_2 dissociation into CO and O [23].

(4) Formation of hydroxyl groups. H* generated by CH_4 decomposition could diffuse from the surface of active metal particles to the support under the DRM reaction condition and react with the O* species generated by CO_2 decomposition to form OH species [23].

(5) Syngas formation. In the final step, syngas is formed as a result of a radical recombination.

2.2. Catalyst Deactivation Mechanism

In the DRM reaction, the deactivation of the catalyst is mainly caused by carbon deposition and sintering of the active components.

Carbon deposition is the process of carbon species covering the active sites, reducing the contact between reactants and active metals. Carbon species can be classified into different types based on morphology, properties, and relative deactivation rate. It includes the adsorbed atomic carbon C_α, polymeric carbon filaments C_β, graphitic carbon C_c, and carbon whiskers C_v (Figure 2). C_α is formed from the dissociation of reactants and products of DRM, CO_2, CH_4, and CO on the catalyst. When the temperature is above 250 °C, the generation rate of C_α will exceed its gasification rate and accumulate on the surface. As it accumulates, they react together to convert into C_β. As the temperature continues to rise, C_α and C_β will convert into carbon whiskers C_v and graphite carbon C_c. It is noteworthy that not every kind of carbon species reduces the activity of the catalyst. For example, C_α and C_β can be eliminated by oxidants formed during the reaction with little impact on the catalytic activity. However, at 500–900 °C, the carbon whiskers C_v exhibit thermodynamic stability with a thickness of over 80 atomic diameters, making it difficult to oxidize and remove. In addition, when generating a large amount of C_v, it will cause the active metal components to move and aggregate. Graphite carbon C_c is also difficult to eliminate through oxidation reactions [25]. It will cover the surface of the catalyst, even completely envelop the active sites, block pores, isolate internal active components, and prevent them from contacting reactants, thus deactivating the catalysts. In addition, C_c can also block the reactor, increase the load pressure of the catalytic bed, and damage the structure of the catalyst. In summary, at the typical DRM temperature, 500–900 °C, the main carbon species are carbon whiskers C_v and graphite carbon C_c [25]. Therefore, for Ni-based catalysts in the DRM process, it is crucial to solve the problem of carbon deposition to maintain the activity and stability simultaneously.

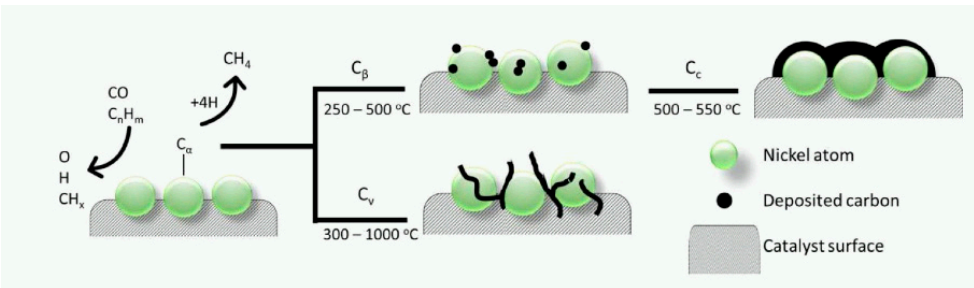

Figure 2. Carbon formation, deposition, and transformation pathways on the Ni-based catalyst [25]. Reprinted with permission from Elsevier, copyright 2019.

Sintering is the migration and agglomeration of the active metal at high temperatures, which reduces the number of active sites, resulting in a decrease in the activity of the catalyst [26]. The oxidation of active metals during the reaction and its reaction with the support or promoters, as well as the collapse of the pore structure of the catalyst support at high temperatures, will also cause catalyst deactivation. Although it is difficult to avoid carbon deposition and sintering of the active components, the above problems can be effectively mitigated by the design and modulation of the catalyst.

Additionally, the possible presence of temperature hysteresis phenomenon in the typical endothermic reaction of DRM could be one of the reasons for deactivation. However, the mechanism of its occurrence is still unclear. Wang et al. [27] studied the hysteresis phenomenon of the Ni/SBA-15 catalyst in the DRM reaction and deeply analyzed the reasons and mechanisms behind this phenomenon (Figure 3). The ignition temperature (T_{ign}) is 425 °C, and the text temperature is 295 °C. At temperatures below T_{ign}, the surface Ni^0 is oxidized to NiO by CO_2 or O in the support, making the reaction difficult to proceed. At T_{ign}, NiO reduction and methane cracking occur simultaneously, generating carbon nanotubes that inhibit the oxidation of Ni^0. When the reaction temperature is higher than T_{ign}, carbon nanotubes generated by methane cracking form a unique catalyst structure with surface Ni, which promotes the catalyst to still have catalytic activity at temperatures lower than T_{ign}. When it is below Text (the activity decreases to 0% at Text), CH_4 cannot continue to reduce NiO, the cycle between the NiO and Ni is broken, and the catalyst is deactivated [27] (Figure 3).

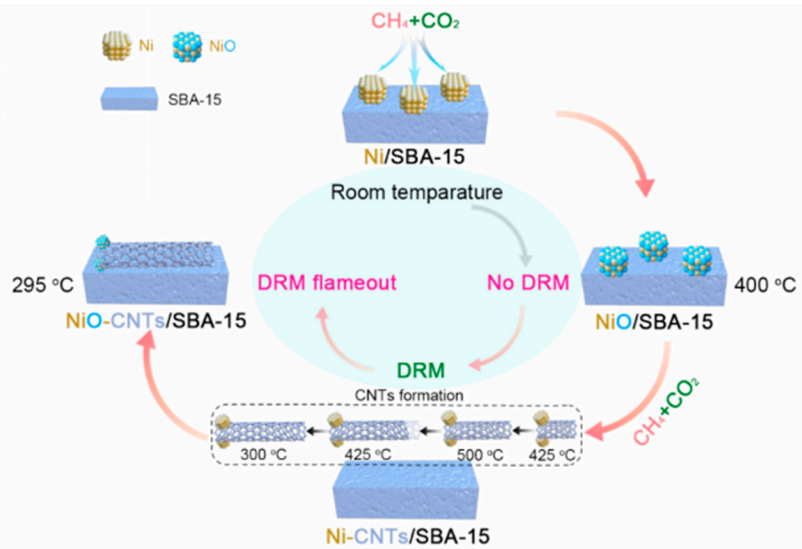

Figure 3. Schematic diagram of the variation in catalysts in the DRM hysteresis reaction under different conditions [27]. Reprinted with permission from Elsevier, copyright 2023.

3. Regulation of Carbon Deposition on Ni-Based DRM Catalysts

Many strategies, such as structural and electronic engineering, are employed to adjust the properties of the catalysts. For the control of carbon deposition on Ni-based DRM catalysts, the design includes the following aspects.

3.1. Regulation of Active Metals

3.1.1. Ni Configuration

The configuration of Ni matters during the catalytic reaction [28,29]. The zero-valenced Ni centers, namely metallic Ni, are required for DRM, while the limited amount of metallic Ni minimizes carbon deposition [30–32]. Wang et al. [15] found that for the Ni-Zr/SiO_2 catalyst, the Ni^0 species was oxidized to a NiO species under the reaction conditions and could not be restored, leading to its deactivation.

The carbon deposition causes the deformation and recombination of the active metal particles. Due to the friction exerted by carbon deposits, the Ni particles in the Ni-based catalyst may become pear-shaped and transfer to elongated conical at high temperatures. In addition, since high Ni dispersion reduces metal sintering and hinders C_v formation, the stability of the catalyst can be enhanced by increasing the dispersion of Ni and adopting the appropriate operating temperature for the Ni-based catalyst. Note that agglomeration and sintering can again increase above an optimal limit of metal dispersion.

3.1.2. Ni Particle Size

The size of Ni particles is another important factor controlling the stability of DRM catalysts. Recently, in order to fully utilize the metal center [33], a series of single-atom catalysts have been developed for DRM applications. Mohcin Akri, et al. [34] designed and prepared a stable Ni single-atom catalyst through interaction with Ce-doped hydroxyapatite (HAP), showing a high activity of DRM and excellent carbon resistance ability. Experimental and computational studies have shown that isolated nickel atoms are inherently carbon-resistant because they have the unique property of activating only the first carbon-hydrogen bond in CH_4, thus avoiding the deep decomposition of methane into deposited carbon species. It was found that the cerium doping of HAP support stabilized the atomically dispersed Ni, which significantly improved the anti-sintering performance of the $0.5Ni_1$/HAP-Ce catalyst. After 65 h reactions, the conversion of CO_2 and CH_4 retains 90% of the initial with a small decrease. The HAP-Ce support has almost no activity towards DRM, indicating that its activity mainly comes from atomically dispersed Ni. The main role of Ce is to stabilize atomically dispersed Ni rather than to inhibit carbon deposition. This observation is consistent with results from recently reported Fe single-atom catalysts catalyzing non-oxidized coupling reactions of CH_4 with ethylene and aromatics [35], in which no carbon deposition was observed. Theoretical calculations also show that the oxide-supported Pt single-atom catalyst can only efficiently activate the first C-H bond in CH_4, matching well with the experimental results [36].

3.1.3. Second Active Metal

As a non-precious metal element, Ni shows high catalytic activity but low anti-deposition ability towards the DRM reaction process. While precious metals (Ru, Rh, Ir, Pd, Pt, etc.) own high activity and good carbon-resistant properties, they are expensive. Therefore, adding a small number of precious metals as co-active components [37] could achieve excellent activity and stability simultaneously with high cost-effectiveness [38]. In general, a large number of active Ni components in Ni-based catalysts migrate to the outside of the pore, causing Ni to sinter and forming large-sized particles. The addition of a second component, such as Pt, can greatly avoid the diffusion of active metals to the outside, decrease the size of metal particles, and reduce the sintering of metal particles in the pore. Recently, Li et al. [39] designed and constructed a highly dispersed Ni-Ir/$MgAl_2O_4$ alloy catalyst for the DRM reaction. Based on the synergistic effect between Ni, Ir, and $MgAl_2O_4$, high catalytic activity and stability were achieved concurrently. Ni is the main activation center of CH_4, while the Ir can effectively utilize the surface carbonates formed by the adsorption of CO_2 on the $MgAl_2O_4$ support to generate active oxygen species, which can further be used for the elimination of the carbon species generated after the activation of CH_4 (Figure 4). Based on the equilibrium mechanism between the active site and carbon deposition, the dynamic balance between carbon deposition and elimination can be achieved by regulating the active site so that the carbon deposition in this system will not continue to increase with the increased reaction time. The optimal Ni_3Ir_6/$MgAl_2O_4$ catalyst achieved near-zero carbon deposition during a 600 h high-temperature DRM reaction [39].

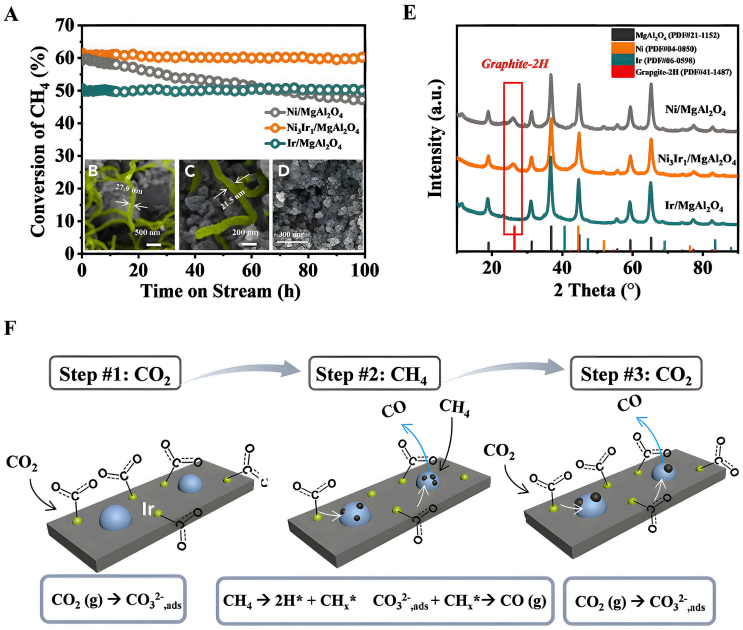

Figure 4. Catalytic performances of Ni-Ir catalysts in DRM and the characterization of spent catalysts [39]. (**A**) CH_4 conversion on $Ni/MgAl_2O_4$, $Ni_3Ir_1/MgAl_2O_4$, and $Ir/MgAl_2O_4$ (reaction conditions for the catalytic test: 650 °C, CH_4/CO_2 = 1/1, GHSV = 40,000 mL g^{-1} h^{-1}, and 1 bar). SEM images of (**B**) $Ni/MgAl_2O_4$, (**C**) $Ni_3Ir_1/MgAl_2O_4$, (**D**) $Ir/MgAl_2O_4$, (**E**) XRD patterns of the spent catalysts. (**F**) The schematic diagram of the mechanism to activate CO_2 with the assistance of carbonate [39]. Reprinted with permission from Elsevier, copyright 2022.

In sum, based on the investigation of the influence of the Ni configuration, the size of the Ni particles, and doped metal components on catalyst stability, it is found that the effective dispersion of Ni and the avoidance of active components sintering can prolong the service life of catalysts.

3.2. Regulation of Supports

The support is generally inert in the DRM reaction. However, it can affect the stability and mechanical strength of the catalyst via the interaction between the active component and the support. Moreover, the surface area, pore structure, thermal stability, oxidation-reducibility, and surface alkalinity of the support can affect the carbon deposition behavior of the Ni-based catalyst [40].

Ni-based DRM catalysts generally use porous oxides as supports, such as metal oxides γ-Al_2O_3 [12,41], SiO_2 [40,42], MgO [43], ZrO_2 [11,44], CeO_2 [45] with rich acidic/alkali sites or good reducibility [46]. The structure, acidity, and alkalinity of the support, defects, and the use of the new catalyst support will affect the carbon deposition [40,42,47,48].

3.2.1. Support Structure

As described above, the support can affect the particle size and dispersion of the active metal in the catalyst and directly affect the activity and stability of the DRM catalysts. For the Ni-based catalysts, the use of a support with a high specific surface area and a finely controlled pore structure can obtain small Ni nanoparticles, improve the dispersion of the active component, prevent the sintering of metal particles, and reduce carbon deposition [40]. Al_2O_3-supported Ni-based catalysts, one of the widely employed DRM catalysts, exhibit a high catalytic activity because of their good structural characteristics, strong metal–support interaction (SMSI) effect, and high dispersion of Ni particles. The porous 3D structure enables the Ni nanoparticles to remain uniformly dispersed in the catalyst. In addition, the formation of the spinel structure $NiAl_2O_4$ during DRM makes the catalyst highly stable. However, the generation of the $NiAl_2O_4$ phase also limits the metal

utilization of the active Ni site, thereby reducing the DRM reactivity. The formed $NiAl_2O_4$ spinel is unstable and can be reduced to Ni during the DRM reaction by a reductive gas mixture of CO and H_2. After adding an appropriate amount of MgO to the Ni@Al_2O_3 catalyst, the spinel structure $MgAl_2O_4$ generated during the reaction also contributes to the resistance to carbon deposition [49].

ZrO_2 is another commonly used support due to its high oxygen storage capacity and high thermodynamic stability [50]. The crystal structure of ZrO_2 is closely related to the catalytic activity and stability of the catalysts [21]. Naeem et al. [51] prepared Ni@Al_2O_3, Ni@CeO_2, and Ni@ZrO_2 using polyol and surfactant-assisted methods. Among these catalysts, Ni@ZrO_2 prepared using the polyol method delivers the highest reactivity, while the Ni@ZrO_2 obtained using the surfactant-assisted method shows the lowest reactivity. This difference in catalytic performance is due to the phase state of ZrO_2. The ZrO_2 of the monoclinic crystal system was mainly prepared using the polyol method, while the ZrO_2 of the cubic crystal system was mainly prepared using the surfactant-assisted method [51]. The former shows better redox properties than the latter and favors the adsorption and activation of CO_2 better, leading to higher reactivity [51].

The distribution of active metal components at different locations of the support also affects carbon deposition. For example, Yan et al. [52] prepared and designed two types of Ni/CeO_2-SiO_2 catalysts, including CeO_2 (Ni/CeO_2-SiO_2-P) in close contact with Ni nanoparticles or CeO_2 (Ni/CeO_2-SiO_2-C) away from the Ni nanoparticles for DRM. Compared with Ni/CeO_2-SiO_2-C, Ni/CeO_2-SiO_2-P exhibits superior low-temperature activity and H_2/CO ratio [52]. At 700 °C, the CO_2 and CH_4 conversion rates of the former (87.3% and 78.5%) were higher than those of the latter (80.5% and 67.8%). Ni/CeO_2-SiO_2-P was stable in long-term tests, while Ni/CeO_2-SiO_2-C showed poor stability, and the activity was significantly reduced within 10 h. The improved performance and stability of the Ni/CeO_2-SiO_2-P resulted from rich reactive oxygen species and more accessible formate species located at the metal-support interface [52] (Figure 5).

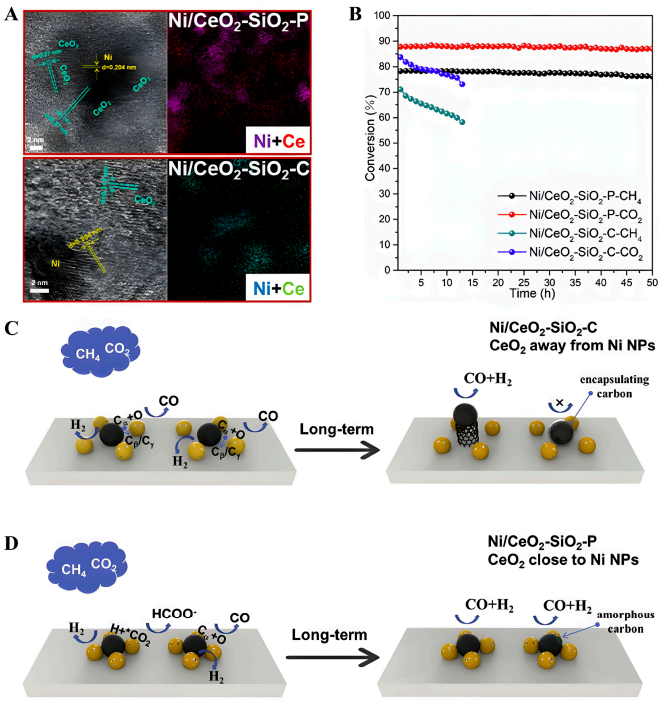

Figure 5. (**A**) TEM images of Ni/CeO_2-SiO_2-C and Ni/CeO_2-SiO_2-P. (**B**) Stability test at 700 °C [52]. (**C**,**D**) Illustration of the reaction pathways of DRM. Reprinted with permission from Elsevier, copyright 2019.

3.2.2. Acidity and Alkalinity of the Support Surface

In the high-temperature DRM process, the support affects the acidity and alkalinity of the catalyst, and the change in acidity and alkalinity further affects the reaction mechanism and carbon deposition. For Ni-based catalysts, the support properties affect the adsorption and dissociation of CO_2 and CH_4 on the catalyst and determine the reaction pathway of DRM [53]. If the inert support (SiO_2) is used as the catalyst support, the reaction follows a single-function pathway, that is, CH_4 and CO_2 are adsorbed and activated on the surface of the active metal, and the inert support is only used as the skeleton of the catalyst, providing large pore volume, good thermal stability, and good dispersibility for the active metal [42,53]. CO_2 is an acid gas, and using an alkaline support may lead to an increase in the adsorption capacity of CO_2. Introducing the Lewis alkali support reduces the formation of deposited carbon and improves stability [54]. As illustrated in Reference [51], the Ni@ZrO_2 prepared using the surfactant-assisted method with high basicity shows better coke-resistant ability but lower reactivity compared with the one prepared by the surfactant-assisted method with low basicity. However, the basic support decreases the adsorption of CH_4 and may reduce the DRM reaction activity. The acidic support reduces the adsorption of CO_2 but promotes the CH_4 adsorption, which may favor the generation of side products to result in increased carbon deposits. When the weakly acidic or weakly basic (CeO_2, La_2O_3) support is employed as the support of the Ni-based catalyst, DRM takes place via a bifunctional reaction pathway, that is, CH_4 is activated on the active metal, and CO_2 is activated on the support or interface [55–57]. Alkaline additives, such as alkali metals, are used to increase the surface alkalinity of the catalyst, thereby accelerating the activation of CO_2 and the gasification of carbon [58].

3.2.3. Support Defects

Surface defects of metal oxides provide a way to stabilize thermodynamically unstable metal atoms and as active sites to promote adsorption and chemical transformation of reactants [21].

For non-redox support Al_2O_3, the surface defects are also used in regulating the catalytic reactivity of reactions. In general, the so-called defect sites on Al_2O_3 are mainly related to the coordination of the unsaturated Al site and the adjacent lattice O atoms. The under-coordinately tricoordinated Al^{3+} sites are closely related to surface dehydroxylation. Zhang et al. [59] proposed a new comprehension of the special role of defect sites on γ-Al_2O_3. Ni/CeO_2-SiO_2 catalyst was prepared using the plasma decomposition method, which is characterized by close contact between the CeO_2 and Ni nanoparticles. In previous work, plasma-decomposed nickel catalysts showed smaller nickel particle sizes, fewer defect sites, and stronger nickel-support interactions compared to thermal decomposed nickel catalysts. The development of the acid etching strategy has been applied to the directional removal of OH groups on the surface of the γ-Al_2O_3, thereby generating the necessary vacancy defects to anchor the active Ni site, and the moderate interaction of Ni with the modified γ-Al_2O_3 support has improved the utilization of Ni. These designed defects promote the adsorption and activation of CO_2 and the activation of CH_4, thus improving the stability and activity of traditional Ni/Al_2O_3 catalysts [59].

Redox oxide supports, such as CeO_2 and TiO_2, have a high concentration of highly reactive oxygen species and unique redox properties ($M^{4+} \leftrightarrow M^{3+}$) [60–66]. The surface defects anchor Ni, forming a strong interaction between the metal and the support, preventing the metal from sintering. Reactive oxygen species can act as local sources or reservoirs of oxygen species, which are involved in reactions that occur on oxide surfaces [23]. The effective barrier for methane activation decreases to 0.15 eV on Ni/CeO_{2-x}(111) compared with 0.9 eV on Ni(111) [67]. Recent studies show that Co-substituted CeO_2 is more stable than Ni-substituted CeO_2 under the DRM reaction conditions at 800 °C. Surface lattice oxygen reactivity plays a vital role in catalytic stability. The vacancy formation is favored in Co-substituted CeO_2 as compared to Ni-substituted CeO_2, leading to a higher availability of surface oxygen in Co-substituted catalyst than Ni-substituted CeO_2 for the reaction [68].

Interfacial metal-$O_{lattice}$ favors the O-assisted CH_4 dissociation, forms CH_xO intermediate, and finally yields CO. The reacted $O_{lattice}$ can be re-supplied by CO_2 dissociation at the metal-CeO_2 interface [69].

It is worth pointing out that recent works mostly use combined strategies to regulate catalyst activity and stability jointly. For example, Li et al. [70] claim that the high Ni dispersion, intensified Ni–support interaction, the enlarged oxygen vacancies, the increased *t*-ZrO_2 content, and enhanced reducibility of NiO led by oxygen vacancies co-boost the superior catalytic activity and stability of the developed LA-Ni/ZrO_2 catalyst. Although a larger amount of coke is deposited on the spent LA-Ni/ZrO_2 catalyst in comparison with that on the spent Ni/ZrO_2, the developed LA-Ni/ZrO_2 illustrates much higher catalytic stability than Ni/ZrO_2, ascribed to the superior thermal sintering resistance of Ni nanoparticles and the different coke morphologies induced by enforced interaction of Ni and the ZrO_2 support [70]. Similarly, among a series of Ni-$Ce_xZr_{1-x}O_2$ and Ni-$Ce_xTi_{1-x}O_2$ catalysts with varying Ce/Zr and Ce/Ti molar ratios (x = 0, 0.25, 0.5, 0.75, and 1), Ni-$Ce_{0.5}Zr_{0.5}O_2$ and Ni-$Ce_{0.5}Ti_{0.5}O_2$ delivered the highest apparent activity and stability for combined steam and CO_2 reforming of CH_4 in each series due to small Ni particles, strong metal–support interaction, and high oxygen vacancy concentration [71]. Ding et al. [72] also find that doping the optimized amount of cerium (Ce/Mg = 0.12) into Ni/MgO catalyst can improve activity and stability, which are attributed to the easy reducibility of NiO_x species, small Ni particle size, and abundant oxygen vacancies resulting from the doping of cerium.

3.2.4. New Catalyst Support

Employing novel materials, such as MXene, as the support of Ni-based catalysts has also received much attention. For example, MXene is a class of layered two-dimensional (2D) transition metal carbides [73]. Due to its large specific surface area, high conductivity and strong redox properties, and the presence of hydroxyl groups or terminal oxygen on the surface, the multilayer structure of V_2CT_xMXene maintains a certain degree of extension in the environment of inert gas (N_2) and reducing gas (H_2). And in the presence of CO_2 and air, V_2CT_xMXene can be completely oxidized (V_2CT_x is converted to V_2O_5) [74]. After 100 h of reaction, its stability is still very high; no carbon deposition has been found, showing excellent resistance towards carbon deposition. It has the potential to be used as a precursor, support, or catalyst for the DRM reaction [74]. Another 2D support is nitride, such as BN. Because BN has the advantages of high thermal stability, strong chemical inertness, good thermal conductivity, and corrosion resistance, it shows greater application potential than traditional oxides under harsh reaction environments. As expected, BN-supported Ni-based catalysts show good resistance to carbon deposition during DRM [19]. However, due to the inert surface of BN, Ni particles are prone to sintering on the surface of the BN, which leads to an unstable Ni-BN interface. Based on this, a research group first reduced the particle size of Ni particles by reducing the Ni loading (0.3 wt%) to increase the proportion of Ni-BN interfaces and then confined the Ni particles to the edge of BN by functionalizing amorphous SiO_2 generated by functional group decomposition on boron nitride (BN_f), thereby constructing a stable Ni-BN interface. The results show that Ni/BN_f shows excellent resistance to carbon deposition during DRM, and Ni remains in a metallic state after reaction for 10 h. For comparison, under the same DRM conditions, no carbon deposition is observed on the surface of the Ni/BN_f catalyst, while a few deposited carbons are produced on the surface of the Ni/α-Al_2O_3 catalyst. Additionally, under the condition of the CH_4 pyrolysis experiment alone, no obvious carbon deposition is observed on the Ni/BN_f catalyst (Figure 6), while carbon deposition on the Ni/α-Al_2O_3 catalyst surface continues to occur, and deposited carbon covered all surfaces of the catalyst. In situ tests and theoretical calculations show that the catalyst promotes the first C-H cleavage and inhibits the last C-H bond cleavage of CH_4. When CH_4 and CO_2 are injected at the same time, CO_2 preferentially activates on the Ni surfaces. Altogether, it makes the catalyst present excellent resistance to carbon deposition [19].

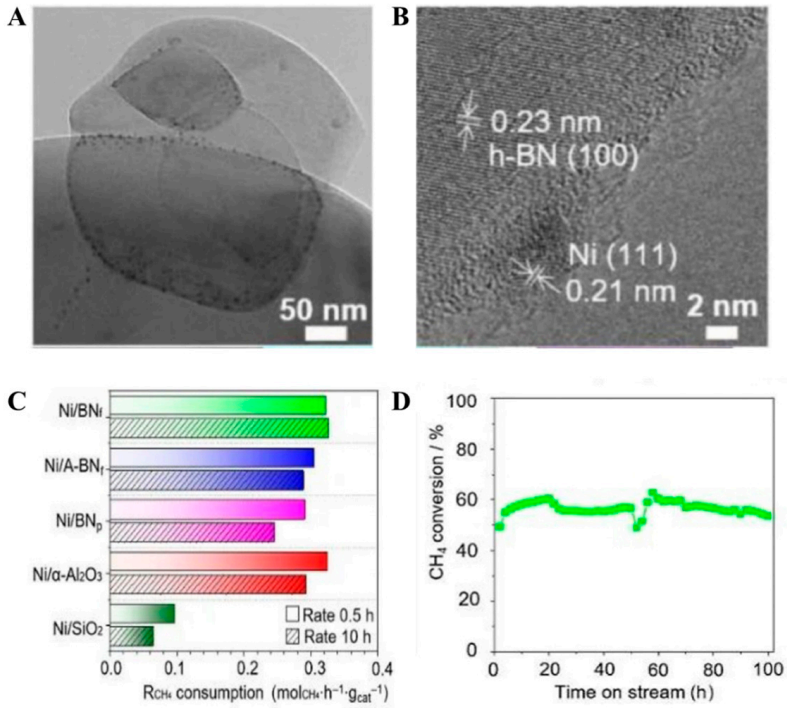

Figure 6. (**A**,**B**) TEM images of the Ni/BN_f and XAS images. (**C**) Activity and (**D**) stability of catalyst [19]. The figures are published on CCS chemistry and are available online [19].

In sum, the carbon deposition behavior of the Ni-based catalyst can be adjusted by the pore structure, oxidation-reducibility, and surface alkalinity of the support.

3.3. Interface Structure Control

The interfacial structure is widely confirmed to influence the properties of the composites [75], such as the resistance towards carbon deposition during Ni-based catalysts catalyzing DRM [76]. Recently, studies have shown that adjusting the interface and strengthening the interaction between Ni and the support play a vital role in the synthesis of efficient and stable Ni-based DRM catalysts. Agglomeration of Ni nanoparticles can be avoided by regulating the SMSI between the metal (Ni) and the support. Compared to bare Ni NPs, the greater the contribution of the Ni–support interface, the stronger the adsorption or activation of the reactants [77]. Stronger Ni–support interactions yield more uniform distribution and smaller Ni nanoparticles, which is conducive to high activity and stability. Jeon et al. [76] propose the strategy of suppressing Ni nanoparticle aggregation during the reduction process via in situ reduction using dry methane (CH_4/CO_2) as the reducing gas. It increases the exposed interface between the Ni and CeO_2 and results in large amounts of the Ni^{3+} phase at the catalyst surface, of which SMSI is dramatically enhanced (Figure 7). SMSI originates from Ni-doped sites on the CeO_2 (denoted as the Ni^{3+} phase). The more Ni^{3+} on the surface, the more SMSI is formed near the exposed Ni nanoparticles, the smaller the size of Ni nanoparticles prepared, and the better the durability and activity. The developed catalyst achieved a methane conversion of 60% for 550 h at a low DRM operating temperature of 600 °C [76].

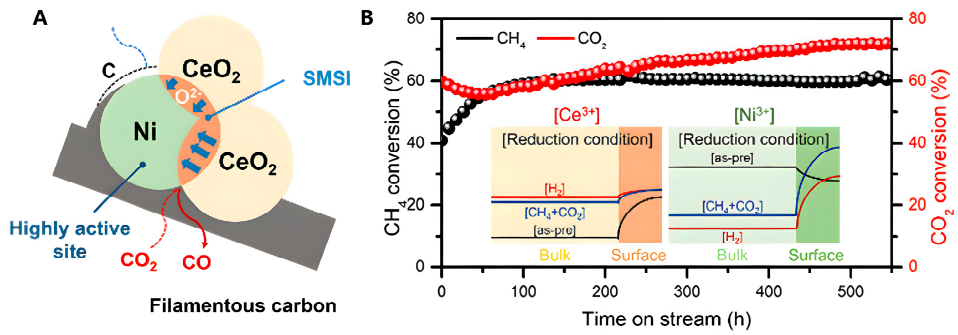

Figure 7. (**A**) Illustration of the formation and role SMSI in anti-coking formation during DRM. (**B**) CH_4 and CO_2 conversion at 600 °C with dry methane ($CH_4/CO_2/N_2$ = 1:1:2) and GHSV of 10,000 h^{-1} of the fabricated catalyst after CH_4/CO_2 reduction. Insert: Scheme of the concentration gradient of the Ni^{3+} and Ce^{3+} fraction at the bulk and surface of the nanoparticles. Reprinted with permission from [76]. Copyright {2022} American Chemical Society.

3.4. Special Structure Design

The configuration of the Ni centers, size of Ni particles, and exposed crystal surface are the key factors affecting its catalytic performance. Because Ni particles are on the surface of the catalyst and are exposed to the reaction stream directly, the supported Ni nanocatalysts prepared by conventional impregnation or precipitation migrate and aggregate during the DRM. Therefore, the design of special structures [78–82], e.g., core-shell [24], to protect metal active centers is the key to improving the stability of the catalysts. Employing this strategy, researchers improve the resistance ability of Ni-based DRM catalysts towards sintering and carbon deposition.

3.4.1. Reverse Metal-on-Oxide

Recently, some research teams innovatively constructed nanostructured oxides on the surface of metals to form reverse oxide-on-metal catalysts [44,64]. Due to the interaction between the oxide and the metal, the oxide formed on the metal surface is a single-layer dispersed, metastable structure, and metal active centers with coordination unsaturated are formed at the oxide-metal boundary, which can efficiently activate O_2, H_2O, and other molecules, and can be successfully used in low-temperature catalytic oxidation, etc. Another group has successfully grown nano-ZrO_2 films on Pt, Cu, Pd, and Ni, denoted as ZrO_2@M (M = Ni, Pt, Cu, Pd), using chemical vapor deposition and applying them to the DRM reaction. This new type of reverse catalyst shows excellent resistance to carbon deposition. It was found that the activity and stability of DRM are closely related to Zr^0. Graphitic deposits are anti-segregated into Ni^0 nanoparticles to provide restored CH_4 adsorption sites and near-surface/dissolved C atoms, which migrate toward the Ni^0/ZrO_2 interface and induce local Zr_xC_y formation. The resulting oxygen-deficient carbidic phase boundary sites assist in kinetically enhanced CO_2 activation toward CO [44,64].

3.4.2. Encapsulated Structure

Encapsulating active metal nanoparticles with a protecting shell, such as a carbon layer or zeolite [83], is an effective way to increase their stability. For Ni-based catalysts, using the zeolite with a special pore structure as the protector is widely employed so that the migration of Ni is inhibited effectively, thereby improving the resistance to carbon deposition. For example, based on this strategy, researchers encapsulate active Ni nanoparticles by the silicon-aluminum MFI zeolite (Ni@HZSM-5) [83]. They further regulate the pore environment of zeolite to enhance the hydrogen spillover so as to keep enough active hydrogen species available around Ni nanoparticles [83]. This facilitates the reduction of CO_2 to CO and suppresses the side reaction of RWGS. In a CO_2-rich atmosphere, the methane on the catalytic material can reduce CO_2 by 2.9 (1 mol of methane reduces 2.9 mol CO_2), which is better than the most advanced super-DRM process reported so far. The CO

yield of 3.9 mol_{CO} $mol_{CH4}{}^{-1}$ on this catalytic material can be carried out for a long time. It is expected to realize the direct conversion and utilization of CO_2-rich natural gas [83].

Similarly, Wang et al. [84] prepared small-sized bimetallic NiCo nanoparticles encapsulated in silicalite-2 (S-2) using the in situ growth method. Elemental segregation is observed during the activation process, in which Ni and Co atoms migrate to the outer surface and center of the NiCo alloy, respectively [84]. The optimal $Ni_{0.2}Co_{0.3}$@S-2 catalyst shows stable and high CH_4 and CO_2 conversion within 100 h without carbon deposition [84]. This localized effect, combined with the precise dynamic balance of carbon and oxygen content on the catalyst surface, makes it have high catalytic performance [84].

In another example, a catalyst of attapulgite-derived MFI (ADM) zeolite-encapsulated Ni-Co alloys was fabricated using a one-pot method. Co in Ni–Co alloys transfers electrons to Ni, forming electron-rich Ni metal sites, which significantly improves the ability of C-H bond cleavage [47]. Meanwhile, the ADM zeolite not only stabilized metallic sites by pore or layer confinement but also offered massive CO_2 adsorption/activation centers. These improve the ability of the anti-sintering and anti-coking formation as well as the superior DRM activity of the optimal $10Ni_1Co$@ADM-0.1 catalyst [47].

Active metal nanoparticles can also be encapsulated using surface coating oxides (e.g., SiO_2, >10 nm). He et al. [85] grew Ni nanoparticles in situ from the MgO–Al_2O_3 matrix and surrounded by a thin layer of 1–2 nm multielement oxide (Ni@NiSiAlMgO_x), and synchronously controlled the size, exposed crystal planes, surface acidity and alkalinity, and redox state of the Ni nanoparticles, thereby improving the stability of Ni catalysts in DRM reactions (Figure 8). The oxide thin layer efficiently isolated and confined the Ni nanoparticles, avoiding fast C–C bond formation on an open facet and protecting the Ni nanoparticles from sintering [85]. The appropriately sized Ni particles of around 15 nm balanced the carbon decomposition and elimination rates. The nearby basic sites assist CO_2 adsorption and accelerate carbon elimination. The cooperative metallic Ni and the surficial MEO thin layer containing Ni^{2+} enhanced the anti-sintering of Ni@NiSiAlMgO_x in a redox atmosphere of MDR [85].

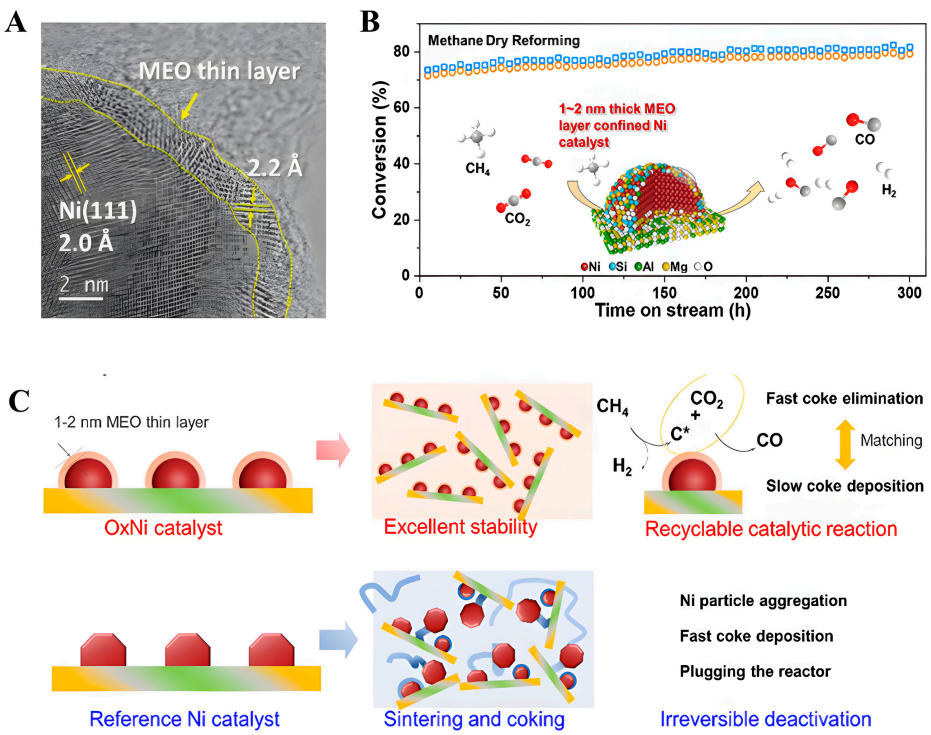

Figure 8. (**A**) High–resolution STEM image; (**B**) long–term stability tests of Ni@NiSiAlMgO_x at 673 and 873 K; (**C**) schematic representation of the MEO thin layer–confined and –stabilized Ni catalyst and the reference sample. Reprinted with permission from [85]. Copyright {2021} American Chemical Society.

As summarized in Table 2, the $CO:H_2$ mole ratio is less than 1 due to the presence of side reaction, the conversion rate of CO_2 is usually higher than that of CH_4, and the stability can reach 550 h. In addition to the above regulation strategies, the stability of the catalyst can also be improved using other strategies, which are not discussed in this review in detail.

Table 2. Performances of the Ni-based catalysts toward DRM.

Catalyst	Reaction Condition	H_2/CO	CO_2 Conversion Rate	CH_4 Conversion Rate	Stability (h)	Ref.
Ni@NiSiAlMgO$_x$	T = 873 K, $pCH_4:CO_2$ = 1:1, GHSV = 30,000 mL g_{cat}^{-1} h^{-1}	0.78	40%	31%	~320	[85]
Ni-cerium oxide nanocatalysts	T = 873.15 K, $pCH_4:CO_2:N_2$ = 1:1:2, GHSV = 10,000 h^{-1}	N.A.	60%	40%	550	[76]
Ni/BN$_f$	T = 1023.15 K, $pCH_4:CO_2$ = 1:1, WHSV = 25,000 mL g^{-1} h^{-1}	0.90	N.A.	60%	100	[19]
Ni/CeO$_2$-SiO$_2$-C	T = 973.15 K, $pCH_4:CO_2:Ar$ = 1:1:2, GHSV = 48,000 mL g^{-1} h^{-1}	0.85	80.5%	67.8%	50	[52]
Ni/CeO$_2$-SiO$_2$-P	T = 973.15 K, $pCH_4:CO_2:Ar$ = 1:1:2, GHSV = 48,000 mL g^{-1} h^{-1}	0.89	87.3%	78.5%	50	[52]
Ni/MgAl$_2$O$_4$	T = 923.15 K, $pCH_4:CO_2$ = 1:1, GHSV = 40,000 mL g^{-1} h^{-1}	0.96	71.5%	59.4%	100	[39]
Ni$_3$Ir$_1$/MgAl$_2$O$_4$	T = 923.15 K, $pCH_4:CO_2$ = 1:1, GHSV = 40,000 mL g^{-1} h^{-1}	0.97	73.0%	61.0%	100	[39]
Ir/MgAl$_2$O$_4$	T = 923.15 K, $pCH_4:CO_2$ = 1:1, GHSV = 40,000 mL g^{-1} h^{-1}	0.94	63.6%	50.2%	100	[39]

4. Conclusions and Outlook

The rapid carbon deposition and catalyst sintering induced by high reaction temperature limit the industrial applications of Ni-based catalysts toward DRM reaction. In this review, the mechanisms of reaction and deactivation during DRM reaction are analyzed, and the influencing factors and possible solutions regarding the stability of Ni-based catalysts are summarized. The catalytic activity and stability are co-affected by the active metal, support, interface, etc. The stability of the catalyst can be improved by multi-scale regulation. The metal dispersion is related to stability, which has an optimal limit. Increasing the surface basicity of the support could favor the activation of CO_2 and consequently inhibit carbon deposition on the catalyst. The protection of active centers by the construction of special structures, e.g., encapsulating Ni by oxides, can also improve the stability of catalysts.

Future research can focus on the following aspects: (1) Develop new preparation methods of catalysts to increase the dispersion of Ni particles on the support and adjust the interaction between the metal and the support; (2) increase the number of adsorbed oxygen species on the catalyst surface by the release of partial lattice oxygen, and promote the combination of adsorbed oxygen with adsorbed carbon to form CO, eliminating carbon deposition on the catalyst surface; (3) couple to the reaction of CO hydrogenation, modifying the reaction thermodynamically.

This review provides guidance for the rational design of stable Ni-based catalysts in the industrial application of DRM.

Author Contributions: Conceptualization, M.W. and X.S.; formal analysis, M.W.; investigation, M.W. and X.S.; resources, M.W. and X.S.; writing—original draft preparation, M.W.; writing—review and editing, X.S.; supervision, X.S. All authors have read and agreed to the published version of the manuscript.

Funding: This research was funded by the Shanghai Natural Science Foundation, grant number 23ZR1425500, the foundation of the National Key Laboratory of High Efficiency and Low Carbon Utilization of Coal, grant number Grant No. J23-24-603, Shanghai Local Universities Capacity Building Project of Science and Technology Innovation Action Program, grant number 21010501700, Class III Peak Discipline of Shanghai—Materials Science and Engineering (High-Energy Beam Intelligent Processing and Green Manufacturing).

Institutional Review Board Statement: Not applicable.

Informed Consent Statement: Not applicable.

Data Availability Statement: Not applicable.

Conflicts of Interest: The authors declare no conflicts of interest.

References

1. Meng, C.; Zhao, G.; Shi, X.-R.; Chen, P.; Liu, Y.; Lu, Y. Oxygen-deficient metal oxides supported nano-intermetallic $InNi_3C_{0.5}$ toward efficient CO_2 hydrogenation to methanol. *Sci. Adv.* **2021**, *7*, eabi6012. [CrossRef] [PubMed]
2. Meng, C.; Zhao, G.; Shi, X.-R.; Nie, Q.; Liu, Y.; Lu, Y. Electronic modulation of $InNi_3C_{0.5}/Fe_3O_4$ by support precursor toward efficient CO_2 hydrogenation to methanol. *Appl. Catal. B* **2022**, *316*, 121699. [CrossRef]
3. Zhu, J.; Zhao, G.; Meng, C.; Chen, P.; Shi, X.-R.; Lu, Y. Superb Ni-foam-structured nano-intermetallic $InNi_3C_{0.5}$ catalyst for hydrogenation of dimethyl oxalate to ethylene glycol. *Chem. Eng. J.* **2021**, *426*, 130857. [CrossRef]
4. Chen, P.; Zhao, G.; Shi, X.-R.; Zhu, J.; Ding, J.; Lu, Y. Nano-Intermetallic $InNi_3C_{0.5}$ Compound Discovered as a Superior Catalyst for CO_2 Reutilization. *iScience* **2019**, *17*, 315–324. [CrossRef] [PubMed]
5. Liu, M.; Wu, Z.; Kong, X.; Zhang, X.; Tan, L.; Guo, H.; Li, C.-J. One-pot synthesis of toluene from methane and methanol catalyzed by GaN nanowire. *Nano Res.* **2023**, *16*, 6512–6516. [CrossRef]
6. Zhang, X.; Witte, J.; Schildhauer, T.; Bauer, C. Life cycle assessment of power-to-gas with biogas as the carbon source. *Sustain. Energy Fuels* **2020**, *4*, 1427–1436. [CrossRef]
7. Palmer, C.; Upham, D.C.; Smart, S.; Gordon, M.J.; Metiu, H.; McFarland, E.W. Dry reforming of methane catalysed by molten metal alloys. *Nat. Catal.* **2020**, *3*, 83–89. [CrossRef]
8. Kawi, S.; Kathiraser, Y.; Ni, J.; Oemar, U.; Li, Z.; Saw, E.T. Progress in Synthesis of Highly Active and Stable Nickel-Based Catalysts for Carbon Dioxide Reforming of Methane. *ChemSusChem* **2015**, *8*, 3556–3575. [CrossRef]
9. Sheng, K.; Luan, D.; Jiang, H.; Zeng, F.; Wei, B.; Pang, F.; Ge, J. NixCoy Nanocatalyst Supported by ZrO_2 Hollow Sphere for Dry Reforming of Methane: Synergetic Catalysis by Ni and Co in Alloy. *ACS Appl. Mater. Interfaces* **2019**, *11*, 24078–24087. [CrossRef]
10. Yu, Y.-X.; Yang, J.; Zhu, K.-K.; Sui, Z.-J.; Chen, D.; Zhu, Y.-A.; Zhou, X.-G. High-Throughput Screening of Alloy Catalysts for Dry Methane Reforming. *ACS Catal.* **2021**, *11*, 8881–8894. [CrossRef]
11. Dou, J.; Zhang, R.; Hao, X.; Bao, Z.; Wu, T.; Wang, B.; Yu, F. Sandwiched SiO_2@Ni@ZrO_2 as a coke resistant nanocatalyst for dry reforming of methane. *Appl. Catal. B* **2019**, *254*, 612–623. [CrossRef]
12. Li, Y.; Wang, Q.; Cao, M.; Li, S.; Song, Z.; Qiu, L.; Yu, F.; Li, R.; Yan, X. Structural evolution of robust Ni_3Fe_1 alloy on Al_2O_3 in dry reforming of methane: Effect of iron-surplus strategy from Ni_1Fe_1 to Ni_3Fe_1. *Appl. Catal. B* **2023**, *331*, 122669. [CrossRef]
13. Li, J.; Croiset, E.; Ricardez-Sandoval, L. Effect of Metal–Support Interface During CH_4 and H_2 Dissociation on Ni/γ-Al_2O_3: A Density Functional Theory Study. *J. Phys. Chem. C* **2013**, *117*, 16907–16920. [CrossRef]
14. Xu, Y.; Li, J.; Jiang, F.; Xu, Y.; Liu, B.; Liu, X. Insight into the anti-coking ability of NiM/SiO_2 (M=ZrO_2, Ru) catalyst for dry reforming of CH_4 to syngas. *Int. J. Hydrogen Energy* **2022**, *47*, 2268–2278. [CrossRef]
15. Wang, Y.; Yao, L.; Wang, Y.; Wang, S.; Zhao, Q.; Mao, D.; Hu, C. Low-Temperature Catalytic CO_2 Dry Reforming of Methane on Ni-Si/ZrO_2 Catalyst. *ACS Catal.* **2018**, *8*, 6495–6506. [CrossRef]
16. Köpfle, N.; Götsch, T.; Grünbacher, M.; Carbonio, E.A.; Hävecker, M.; Knop-Gericke, A.; Schlicker, L.; Doran, A.; Kober, D.; Gurlo, A.; et al. Zirconium-Assisted Activation of Palladium To Boost Syngas Production by Methane Dry Reforming. *Angew. Chem. Int. Ed.* **2018**, *57*, 14613–14618. [CrossRef] [PubMed]
17. Wang, M.; Xiang, Y.; Chen, W.; Wu, S.; Zhu, Z.-Z.; Cao, X. $SiFeN_6$-graphene: A promising dual-atom catalyst for enhanced CO_2-to-CH_4 conversion. *Appl. Surf. Sci.* **2024**, *643*, 158724. [CrossRef]
18. Wang, P.; Shi, X.-R.; Zhang, Y.; Wei, M. The influence of Co nucleation in Co-Ni single atom alloy on low-temperature methane dry reforming with DFT simulations and microkinetic modeling. *Mol. Catal.* **2023**, *549*, 113515. [CrossRef]
19. Deng, J.; Gao, M.; Hasegawa, J.; Zhang, X.; Wang, A.; Chen, A.; Zhang, D. Unravelling the Anomalous Coking Resistance over Boron Nitride-Supported Ni Catalysts for Dry Reforming of Methane. *CCS Chem.* **2023**, *5*, 2111–2124. [CrossRef]
20. Chen, S.; Zaffran, J.; Yang, B. Descriptor Design in the Computational Screening of Ni-Based Catalysts with Balanced Activity and Stability for Dry Reforming of Methane Reaction. *ACS Catal.* **2020**, *10*, 3074–3083. [CrossRef]
21. Shi, X.R.; Wang, P.; Jing, C.; Wu, K.; Xu, S.; Klötzer, B. The formation of O vacancy on ZrO_2/Pd and its effect on methane dry reforming: Insights from DFT and microkinetic modeling. *Appl. Surf. Sci.* **2023**, *619*, 156679. [CrossRef]
22. Das, S.; Bhattar, S.; Liu, L.; Wang, Z.; Xi, S.; Spivey, J.J.; Kawi, S. Effect of Partial Fe Substitution in $La_{0.9}Sr_{0.1}$ NiO_3 Perovskite-Derived Catalysts on the Reaction Mechanism of Methane Dry Reforming. *ACS Catal.* **2020**, *10*, 12466–12486. [CrossRef]

23. Laosiripojana, N.; Sutthisripok, W.; Assabumrungrat, S. Synthesis gas production from dry reforming of methane over CeO_2 doped Ni/Al_2O_3: Influence of the doping ceria on the resistance toward carbon formation. *Chem. Eng. J.* **2005**, *112*, 13–22. [CrossRef]
24. Das, S.; Ashok, J.; Bian, Z.; Dewangan, N.; Wai, M.H.; Du, Y.; Borgna, A.; Hidajat, K.; Kawi, S. Silica–Ceria sandwiched Ni core–shell catalyst for low temperature dry reforming of biogas: Coke resistance and mechanistic insights. *Appl. Catal. B* **2018**, *230*, 220–236. [CrossRef]
25. Abdulrasheed, A.; Jalil, A.A.; Gambo, Y.; Ibrahim, M.; Hambali, H.U.; Hamid, M.Y.S. A review on catalyst development for dry reforming of methane to syngas: Recent advances. *Renew. Sustain. Energy Rev.* **2019**, *108*, 175–193. [CrossRef]
26. Liang, Y.; Douthwaite, M.; Huang, X.; Zhao, B.; Tang, Q.; Liu, L.; Dong, J. Zero-oxidation state precursor assisted fabrication of highly dispersed and stable Pt catalyst for chemoselective hydrogenation of α,β-unsaturated aldehydes. *Nano Res.* **2023**, *16*, 6085–6093. [CrossRef]
27. Wang, S.; Wang, Y.; Yao, L.; Hu, C. Temperature hysteresis in dry reforming of methane on Ni/SBA-15 catalyst: Low temperature activity originated from the synergy of Ni^0 and carbon nanotubes. *Appl. Catal. B* **2023**, *333*, 122756. [CrossRef]
28. Zhang, M.; Ding, L.; Zheng, J.; Liu, L.; Alsulami, H.; Kutbi, M.A.; Xu, J. Surface modification of carbon fibers with hydrophilic Fe_3O_4 nanoparticles for nickel-based multifunctional composites. *Appl. Surf. Sci.* **2020**, *509*, 145348. [CrossRef]
29. Liu, C.; Shi, X.; Yue, K.; Wang, P.; Zhan, K.; Wang, X.; Xia, B.Y.; Yan, Y. S-Species-Evoked High-Valence $Ni^{2+\delta}$ of the Evolved β-$Ni(OH)_2$ Electrode for Selective Oxidation of 5-Hydroxymethylfurfural. *Adv. Mater.* **2023**, *35*, 2211177. [CrossRef]
30. Rogers, J.L.; Mangarella, M.C.; D'Amico, A.D.; Gallagher, J.R.; Dutzer, M.R.; Stavitski, E.; Miller, J.T.; Sievers, C. Differences in the Nature of Active Sites for Methane Dry Reforming and Methane Steam Reforming over Nickel Aluminate Catalysts. *ACS Catal.* **2016**, *6*, 5873–5886. [CrossRef]
31. Sumi, T.; Murata, D.; Kitamura, H.; Kubota, S.; Miyake, K.; Uchida, Y.; Miyamoto, M.; Nishiyama, N. Formation of Ni Species Anchored on a Silicalite-1 Zeolite Framework as a Catalyst with High Coke Deposition Resistance on Dry Reforming of Methane. *Cryst. Growth Des.* **2023**, *23*, 3308–3313. [CrossRef]
32. Manabayeva, A.M.; Mäki-Arvela, P.; Vajglová, Z.; Martinéz-Klimov, M.; Tirri, T.; Baizhumanova, T.S.; Grigor'eva, V.P.; Zhumabek, M.; Aubakirov, Y.A.; Simakova, I.L.; et al. Dry Reforming of Methane over Ni–Fe–Al Catalysts Prepared by Solution Combustion Synthesis. *Ind. Eng. Chem. Res.* **2023**, *62*, 11439–11455. [CrossRef]
33. Gu, Y.; Cao, Z.; Zhao, M.; Xu, Y.; Lu, N. Single-Atom Fe Nanozyme with Enhanced Oxidase-like Activity for the Colorimetric Detection of Ascorbic Acid and Glutathione. *Biosensors* **2023**, *13*, 487. [CrossRef] [PubMed]
34. Akri, M.; El Kasmi, A.; Batiot-Dupeyrat, C.; Qiao, B. Highly Active and Carbon-Resistant Nickel Single-Atom Catalysts for Methane Dry Reforming. *Catalysts* **2020**, *10*, 630. [CrossRef]
35. Guo, X.; Fang, G.; Li, G.; Ma, H.; Fan, H.; Yu, L.; Ma, C.; Wu, X.; Deng, D.; Wei, M.; et al. Direct, nonoxidative conversion of methane to ethylene, aromatics, and hydrogen. *Science* **2014**, *344*, 616–619. [CrossRef]
36. Akri, M.; Zhao, S.; Li, X.; Zang, K.; Lee, A.F.; Isaacs, M.A.; Xi, W.; Gangarajula, Y.; Luo, J.; Ren, Y.; et al. Atomically dispersed nickel as coke-resistant active sites for methane dry reforming. *Nat. Commun.* **2019**, *10*, 5181. [CrossRef]
37. Gould, T.D.; Montemore, M.M.; Lubers, A.M.; Ellis, L.D.; Weimer, A.W.; Falconer, J.L.; Medlin, J.W. Enhanced dry reforming of methane on Ni and Ni-Pt catalysts synthesized by atomic layer deposition. *Appl. Catal. A Gen.* **2015**, *492*, 107–116. [CrossRef]
38. Wang, G.; Liang, Y.; Song, J.; Li, H.; Zhao, Y. Study on High Activity and Outstanding Stability of Hollow-NiPt@SiO_2 Core–Shell Structure Catalyst for DRM Reaction. *Front. Chem.* **2020**, *8*, 220. [CrossRef]
39. Li, H.; Hao, C.; Tian, J.; Wang, S.; Zhao, C. Ultra-durable Ni-Ir/$MgAl_2O_4$ catalysts for dry reforming of methane enabled by dynamic balance between carbon deposition and elimination. *Chem. Catal.* **2022**, *2*, 1748–1763. [CrossRef]
40. Zhang, Y.; Zhang, G.; Liu, J.; Li, T.; Wang, Y.; Zhao, Y.; Li, G.; Zhang, Y. Dry reforming of methane over Ni/SiO_2 catalysts: Role of support structure properties. *Fuel* **2023**, *340*, 127490. [CrossRef]
41. Fakeeha, A.H.; Ibrahim, A.A.; Arafat, Y.; Atia, H.; Abasaeed, A.E.; Al-Fatesh, A.S. Iridium promoted Ni-Co/Al_2O_3-ZrO_2 catalyst for dry reforming of methane. *Can. J. Chem. Eng.* **2018**, *96*, 955–960. [CrossRef]
42. Song, Q.; Ran, R.; Wu, X.; Si, Z.; Weng, D. Dry reforming of methane over Ni catalysts supported on micro- and mesoporous silica. *J. CO2 Util.* **2023**, *68*, 102387. [CrossRef]
43. Zeng, F.; Zhang, J.; Xu, R.; Zhang, R.; Ge, J. Highly dispersed Ni/MgO-mSiO_2 catalysts with excellent activity and stability for dry reforming of methane. *Nano Res.* **2022**, *15*, 5004–5013. [CrossRef]
44. Haug, L.; Thurner, C.; Bekheet, M.F.; Ploner, K.; Bischoff, B.; Gurlo, A.; Kunz, M.; Sartory, B.; Penner, S.; Klötzer, B. Pivotal Role of Ni/ZrO_2 Phase Boundaries for Coke-Resistant Methane Dry Reforming Catalysts. *Catalysts* **2023**, *13*, 804. [CrossRef]
45. Odedairo, T.; Chen, J.; Zhu, Z. Metal–support interface of a novel Ni–CeO_2 catalyst for dry reforming of methane. *Catal. Commun.* **2013**, *31*, 25–31. [CrossRef]
46. Gao, X.; Lin, W.; Ge, Z.; Ge, H.; Kawi, S. Modification Strategies of Ni-Based Catalysts with Metal Oxides for Dry Reforming of Methane. *Methane* **2022**, *1*, 139–157. [CrossRef]
47. Liang, D.; Wang, Y.; Chen, M.; Xie, X.; Li, C.; Wang, J.; Yuan, L. Dry reforming of methane for syngas production over attapulgite-derived MFI zeolite encapsulated bimetallic Ni-Co catalysts. *Appl. Catal. B* **2023**, *322*, 122088. [CrossRef]
48. Chatla, A.; Almanassra, I.W.; Kallem, P.; Atieh, M.A.; Alawadhi, H.; Akula, V.; Banat, F. Dry (CO_2) reforming of methane over zirconium promoted Ni-MgO mixed oxide catalyst: Effect of Zr addition. *J. CO2 Util.* **2022**, *62*, 102082. [CrossRef]

49. Shang, Z.; Li, S.; Li, L.; Liu, G.; Liang, X. Highly active and stable alumina supported nickel nanoparticle catalysts for dry reforming of methane. *Appl Catal. B* **2017**, *201*, 302–309. [CrossRef]
50. Zhang, J.; Lv, Z.; Wang, L.; Guo, Y. Preparation of C–N co-doped zirconia electrospun nanofibers and their humidity sensing properties. *Mater. Adv.* **2022**, *3*, 7265–7271. [CrossRef]
51. Naeem, M.A.; Al-Fatesh, A.S.; Fakeeha, A.H.; Abasaeed, A.E. Hydrogen production from methane dry reforming over nickel-based nanocatalysts using surfactant-assisted or polyol method. *Int. J. Hydrogen Energy* **2014**, *39*, 17009–17023. [CrossRef]
52. Yan, X.; Hu, T.; Liu, P.; Li, S.; Zhao, B.; Zhang, Q.; Jiao, W.; Chen, S.; Wang, P.; Lu, J.; et al. Highly efficient and stable Ni/CeO_2-SiO_2 catalyst for dry reforming of methane: Effect of interfacial structure of Ni/CeO_2 on SiO_2. *Appl. Catal. B* **2019**, *246*, 221–231. [CrossRef]
53. Velty, A.; Corma, A. Advanced zeolite and ordered mesoporous silica-based catalysts for the conversion of CO_2 to chemicals and fuels. *Chem. Soc. Rev.* **2023**, *52*, 1773–1946. [CrossRef]
54. Kim, D.H.; Seo, J.-C.; Kim, Y.J.; Kim, J.; Yoon, S.; Ra, H.; Kim, M.-J.; Lee, K. Ni-Co alloy catalyst derived from $Ni_xCo_y/MgAl_2O_4$ via exsolution method for high coke resistance toward dry reforming of methane. *Catal. Today* **2024**, *425*, 114337. [CrossRef]
55. Singh, S.; Zubenko, D.; Rosen, B.A. Influence of $LaNiO_3$ Shape on Its Solid-Phase Crystallization into Coke-Free Reforming Catalysts. *ACS Catal.* **2016**, *6*, 4199–4205. [CrossRef]
56. Wang, M.; Zhao, T.; Dong, X.; Li, M.; Wang, H. Effects of Ce substitution at the A-site of $LaNi_{0.5}Fe_{0.5}O_3$ perovskite on the enhanced catalytic activity for dry reforming of methane. *Appl. Catal. B* **2018**, *224*, 214–221. [CrossRef]
57. Bonmassar, N.; Bekheet, M.F.; Schlicker, L.; Gili, A.; Gurlo, A.; Doran, A.; Gao, Y.; Heggen, M.; Bernardi, J.; Klötzer, B.; et al. In Situ-Determined Catalytically Active State of $LaNiO_3$ in Methane Dry Reforming. *ACS Catal.* **2020**, *10*, 1102–1112. [CrossRef]
58. Zhang, Z.; Zhang, X.; Zhang, L.; Gao, J.; Shao, Y.; Dong, D.; Zhang, S.; Liu, Q.; Xu, L.; Hu, X. Impacts of alkali or alkaline earth metals addition on reaction intermediates formed in methanation of CO_2 over cobalt catalysts. *J. Energy Inst.* **2020**, *93*, 1581–1596. [CrossRef]
59. Zhang, Y.; Zu, Y.; He, D.; Liang, J.; Zhu, L.; Mei, Y.; Luo, Y. The tailored role of "defect" sites on γ-alumina: A key to yield an efficient methane dry reforming catalyst with superior nickel utilization. *Appl. Catal. B* **2022**, *315*, 121539. [CrossRef]
60. Köpfle, N.; Ploner, K.; Lackner, P.; Götsch, T.; Thurner, C.; Carbonio, E.; Hävecker, M.; Knop-Gericke, A.; Schlicker, L.; Doran, A.; et al. Carbide-Modified Pd on ZrO_2 as Active Phase for CO_2-Reforming of Methane—A Model Phase Boundary Approach. *Catalysts* **2020**, *10*, 1000. [CrossRef]
61. Mayr, L.; Shi, X.; Köpfle, N.; Klötzer, B.; Zemlyanov, D.Y.; Penner, S. Tuning of the copper–zirconia phase boundary for selectivity control of methanol conversion. *J. Catal.* **2016**, *339*, 111–122. [CrossRef]
62. Köpfle, N.; Mayr, L.; Lackner, P.; Schmid, M.; Schmidmair, D.; Götsch, T.; Penner, S.; Kloetzer, B. Zirconium-Palladium Interactions during Dry Reforming of Methane. *ECS Trans.* **2017**, *78*, 2419–2430. [CrossRef]
63. Bikaljevic, D.; Rameshan, R.; Köpfle, N.; Götsch, T.; Mühlegger, E.; Schlögl, R.; Penner, S.; Memmel, N.; Klötzer, B. Structural and kinetic aspects of CO oxidation on ZnO_x-modified Cu surfaces. *Appl. Catal. A Gen.* **2019**, *572*, 151–157. [CrossRef]
64. Haug, L.; Thurner, C.; Bekheet, M.F.; Bischoff, B.; Gurlo, A.; Kunz, M.; Sartory, B.; Penner, S.; Klötzer, B. Zirconium Carbide Mediates Coke-Resistant Methane Dry Reforming on Nickel-Zirconium Catalysts. *Angew. Chem. Int. Ed.* **2022**, *61*, e202213249. [CrossRef]
65. Thalinger, R.; Stöger-Pollach, M.; Hetaba, W.; Feuerbacher, M.; Klötzer, B.; Penner, S. Electron microscopy investigations of metal-support interaction effects in M/Y_2O_3 and M/ZrO_2 thin films (M = Cu, Ni). *Mater. Chem. Phys.* **2013**, *143*, 167–177. [CrossRef]
66. Wolfbeisser, A.; Klötzer, B.; Mayr, L.; Rameshan, R.; Zemlyanov, D.; Bernardi, J.; Föttinger, K.; Rupprechter, G. Surface modification processes during methane decomposition on Cu-promoted Ni–ZrO_2 catalysts. *Catal. Sci. Technol.* **2015**, *5*, 967–978. [CrossRef]
67. Liu, Z.; Grinter, D.C.; Lustemberg, P.G.; Nguyen-Phan, T.; Zhou, Y.; Luo, S.; Waluyo, I.; Crumlin, E.J.; Stacchiola, D.J.; Zhou, J.; et al. Dry Reforming of Methane on a Highly-Active Ni-CeO_2 Catalyst: Effects of Metal-Support Interactions on C−H Bond Breaking. *Angew. Chem.* **2016**, *128*, 7581–7585. [CrossRef]
68. Yadav, P.K.; Patrikar, K.; Mondal, A.; Sharma, S. Ni/Co in and on CeO_2: A comparative study on the dry reforming reaction. *Sustain. Energy Fuels* **2023**, *7*, 3853–3870. [CrossRef]
69. Shen, D.; Li, Z.; Shan, J.; Yu, G.; Wang, X.; Zhang, Y.; Liu, C.; Lyu, S.; Li, J.; Li, L. Synergistic Pt-CeO_2 interface boosting low temperature dry reforming of methane. *Appl. Catal. B* **2022**, *318*, 121809. [CrossRef]
70. Li, W.; Zhao, Z.; Ding, F.; Guo, X.; Wang, G. Syngas Production via Steam–CO_2 Dual Reforming of Methane over LA-Ni/ZrO_2 Catalyst Prepared by L-Arginine Ligand-Assisted Strategy: Enhanced Activity and Stability. *ACS Sustain. Chem. Eng.* **2015**, *3*, 3461–3476. [CrossRef]
71. Zhao, Y.; Qi, L.; Cheng, Z.; Zhou, Z. Syngas Production via Combined Steam and Carbon Dioxide Reforming of Methane over Ni-$Ce_xM_{1-x}O_2$(M = Ti or Zr) Catalysts. *Ind. Eng. Chem. Res.* **2022**, *61*, 12978–12988. [CrossRef]
72. Ding, X.; Yang, Y.; Li, Z.; Huang, P.; Liu, X.; Guo, Y.; Wang, Y. Engineering a Nickel–Oxygen Vacancy Interface for Enhanced Dry Reforming of Methane: A Promoted Effect of CeO_2 Introduction into Ni/MgO. *ACS Catal.* **2023**, *13*, 15535–15545. [CrossRef]
73. Liu, J.; Wang, F.; Guo, R.; Liu, Y.; Zhang, M.; Sunarso, J.; Liu, D. Size-regulated co-doped hetero-interfaced 3D honeycomb MXene as high performance electromagnetic absorber with anti-corrosion performance. *Appl. Surf. Sci.* **2023**, *645*, 158846. [CrossRef]

74. Wysocka, I.; Karczewski, J.; Gołąbiewska, A.; Łapiński, M.; Cieślik, B.M.; Maciejewski, M.; Kościelska, B.; Rogala, A. Nickel phase deposition on V_2CT_x/V_2AlC as catalyst precursors for a dry methane reforming: The effect of the deposition method on the morphology and catalytic activity. *Int. J. Hydrogen Energy* **2023**, *48*, 10922–10940. [CrossRef]
75. Shi, X.-R.; Zhang, Y.; Zong, S.; Gu, W.; Ma, P.; Lu, N. Interaction of Ethylene with Ir_n (n = 1–10): From Bare Clusters to γ-Al_2O_3-Supported Nanoparticles. *Nanomaterials* **2019**, *9*, 331. [CrossRef]
76. Jeon, O.S.; Lee, H.; Lee, K.S.; Paidi, V.K.; Ji, Y.; Kwon, O.C.; Kim, J.P.; Myung, J.H.; Park, S.Y.; Yoo, Y.J.; et al. Harnessing Strong Metal-Support Interaction to Proliferate the Dry Reforming of Methane Performance by in Situ Reduction. *ACS Appl. Mater. Interfaces* **2022**, *14*, 12140–12148. [CrossRef]
77. Sun, Y.; Liu, F.; Wang, X.; Lu, K.; Liu, X.; Huang, Y.; Yu, F.; Chen, Y. Highly selective CO_2 electroreduction to CO by the synergy between Ni–N–C and encapsulated Ni nanoparticles. *Dalton Trans.* **2023**, *52*, 928–935. [CrossRef]
78. Zhang, R.; Lu, N.; Zhang, J.; Yan, R.; Li, J.; Wang, L.; Wang, N.; Lv, M.; Zhang, M. Ultrasensitive aptamer-based protein assays based on one-dimensional core-shell nanozymes. *Biosens. Bioelectron.* **2020**, *150*, 111881. [CrossRef]
79. He, X.; Xie, S.; Xu, J.; Yin, X.-B.; Zhang, M. Reactive Template-Engaged Synthesis of NiS_x/MoS_2 Nanosheets Decorated on Hollow and Porous Carbon Microtubes with Optimal Electronic Modulation toward High-Performance Enzyme-like Performance. *Inorg. Chem.* **2023**, *62*, 8033–8042. [CrossRef]
80. Yang, L.; Jin, Z.; Zheng, J.; Zhang, B.; Xu, J.; Yin, X.-B.; Zhang, M. In Situ Construction of Co-MoS_2/Pd Nanosheets on Polypyrrole-Derived Nitrogen-Doped Carbon Microtubes as Multifunctional Catalysts with Enhanced Catalytic Performance. *Inorg. Chem.* **2022**, *61*, 542–553. [CrossRef]
81. Yang, L.; He, X.; Xu, J.; Yin, X.-B.; Zhang, M. Construction of hierarchical Co, Fe Co-doped MoS_2/polypyrrole heterostructure as an efficient bifunctional catalyst for enzyme-like and nitrophenol catalysis. *Colloids Surf. A Physicochem. Eng. Asp.* **2022**, *655*, 130225. [CrossRef]
82. Xiao, Y.; Gong, W.; Zhao, M.; Zhang, M.; Lu, N. Surface-engineered prussian blue nanozymes as artificial receptors for universal pattern recognition of metal ions and proteins. *Sens. Actuators B Chem.* **2023**, *390*, 134006. [CrossRef]
83. Zhu, Q.; Zhou, H.; Wang, L.; Wang, L.; Wang, C.; Wang, H.; Fang, W.; He, M.; Wu, Q.; Xiao, F.-S. Enhanced CO_2 utilization in dry reforming of methane achieved through nickel-mediated hydrogen spillover in zeolite crystals. *Nat. Catal.* **2022**, *5*, 1030–1037. [CrossRef]
84. Wang, J.; Fu, Y.; Kong, W.; Li, S.; Yuan, C.; Bai, J.; Chen, X.; Zhang, J.; Sun, Y. Investigation of Atom-Level Reaction Kinetics of Carbon-Resistant Bimetallic NiCo-Reforming Catalysts: Combining Microkinetic Modeling and Density Functional Theory. *ACS Catal.* **2022**, *12*, 4382–4393. [CrossRef]
85. He, L.; Li, M.; Li, W.-C.; Xu, W.; Wang, Y.; Wang, Y.-B.; Shen, W.; Lu, A.-H. Robust and Coke-free Ni Catalyst Stabilized by 1–2 nm-Thick Multielement Oxide for Methane Dry Reforming. *ACS Catal.* **2021**, *11*, 12409–12416. [CrossRef]